PNAS RESEARCH ARTICLE | CHEMISTRY

Stereospecific control of microbial growth by a combinatoric suite of chiral siderophores

Parker R. Stow[a], Kiefer O. Forsch[b], Emil Thomsen[a], Hiroaki Naka[c], Margo G. Haygood[c], Katherine A. Barbeau[b], and Alison Butler[a,1]

Affiliations are included on p. 7.

Edited by Amy Rosenzweig, Northwestern University, Evanston, IL; received November 14, 2024; accepted January 17, 2025

Bacteria compete for iron by producing small-molecule chelators known as siderophores. The triscatechol siderophores trivanchrobactin and ruckerbactin, produced by *Vibrio campbellii* DS40M4 and *Yersinia ruckeri* YRB, respectively, are naturally occurring diastereomers that form chiral ferric complexes in opposing enantiomeric configurations. Chiral recognition is a hallmark of specificity in biological systems, yet the biological consequences of chiral coordination compounds are relatively unexplored. We demonstrate stereoselective discrimination of microbial growth and iron uptake by chiral Fe(III)–siderophores. The siderophore utilization pathway in *V. campbellii* DS40M4 is stereoselective for Λ-Fe(III)–trivanchrobactin, but not the mismatched Δ-Fe(III)–ruckerbactin diastereomer. Chiral recognition is likely conferred by the stereospecificity of both the outer membrane receptor (OMR) protein FvtA and the periplasmic binding protein (PBP) FvtB, both of which must interact preferentially with the Λ-configured Fe(III)-coordination complexes.

iron | siderophore | chirality | bacteria | coordination-chemistry

Significance

Substrate chirality is central to biological recognition, yet little is known about the biological effects of metal-complex chirality in naturally occurring coordination complexes. Here, we investigate the effects of chirality in a suite of diastereomeric triscatechol siderophores, the first reported example of a biological combinatoric ligand set encoded within microbial genomes. The diastereomeric siderophores coordinate Fe(III) in opposing enantiomeric stereospecificity. Microbial growth maintains a stringent preference for Λ configured Fe(III)–triscatecholate compounds, whereas the Δ Fe(III)–triscatecholate compounds do not support growth, suggesting iron-privatization may be driven through tuning the stereochemistry of the siderophore and the resultant Fe(III)-complex. Metal-based chirality may play an essential role in the biological uptake pathways of other diastereomeric pairs of siderophores and known metal-binding natural products.

Bacteria require iron to grow, yet iron(III) is often not readily available due to its low solubility in aqueous aerobic environments (1, 2). Available iron(III) is further curtailed intracellularly through sequestration by iron-binding proteins—an important factor in host–pathogen interactions (3, 4). Consequently, iron is an object of competition among microbes, substantiated by the diversity of microbial iron-acquisition pathways which have evolved in parallel (4, 5). Many bacteria produce siderophores—organic ligands that coordinate Fe(III) with high affinity—to facilitate iron uptake and to confer a growth advantage against competing microorganisms (6). The structures of hundreds of siderophores are known with widely varying molecular weights and structural features, which principally incorporate three bidentate oxygen chelating groups to coordinate Fe(III). In the classic paradigm, siderophore-mediated iron uptake is orchestrated by a suite of proteins with exquisite specificity toward the endogenous siderophore (1). Gram-negative bacteria express outer membrane receptor proteins (OMR) which recognize and transport their native Fe(III)–siderophore complexes across the outer membrane. Subsequently, periplasmic binding proteins (PBPs), in concert with a suite of ABC transport proteins, translocate the Fe(III)–siderophore across the inner membrane in an energy-dependent process coupled to ATP hydrolysis (7). Cytoplasmic iron release typically involves a reductive pathway to produce Fe(II) which has a reduced affinity for coordination to the siderophore (8). Prior to reduction, cytoplasmic, or periplasmic enzymes may be required to hydrolyze the siderophore backbone, to bring the reduction potential of the Fe(III) complex within the biological window of the ferric reductase enzyme (9). The structural diversity of siderophores and the remarkable specificity of the associated iron-acquisition proteins promotes the privatization of Fe(III), raising the question of how small of a structural change within a siderophore ligand is necessary to deter siderophore piracy among competing microbes.

We recently discovered biosynthetic gene clusters (BGCs) in microbial genomes encoding a family of related diastereomeric pairs of triscatechol siderophores framed on a tri-^{L}Ser scaffold and defined by the presence of the D- and L-cationic amino acids ($^{D/L}$CAA, i.e., Arg, Lys, and Orn). Trivanchrobactin, (DHB-^{D}Arg-^{L}Ser)$_3$ (Fig. 1; DHB is 2,3-dihydroxybenzoic acid), and ruckerbactin, (DHB-^{L}Arg-^{L}Ser)$_3$ (Fig. 1), are diastereomers produced by the marine pathogens *Vibrio campbellii* DS40M4 and *Yersinia ruckeri* YRB, respectively (10, 11). Mediterraneabactin (DHB-^{D}Orn-^{L}Ser)$_3$ and turnerbactin (DHB-^{L}Orn-^{L}Ser)$_3$, produced by the marine microbes *Marinomonas mediterranea* MMB-1 and *Teredinibacter turnerae* T7901, are also diastereomeric (*SI Appendix*, Fig. S1) and are similarly framed on the oligoserine diester scaffold (12, 13). Cyclic trichrysobactin ^{cy}(DHB-^{D}Lys-^{L}Ser)$_3$ and frederiksenibactin (DHB-^{L}Lys-^{L}Ser)$_3$ produced by the plant pathogen *Dickeya chrysanthemi* EC16 and the

Author contributions: P.R.S., H.N., M.G.H., K.A.B., and A.B. designed research; P.R.S., K.O.F., E.T., and H.N. performed research; P.R.S., K.O.F., H.N., M.G.H., K.A.B., and A.B. analyzed data; and P.R.S., K.O.F., E.T., H.N., M.G.H., K.A.B., and A.B. wrote the paper.

The authors declare no competing interest.

This article is a PNAS Direct Submission.

[1]To whom correspondence may be addressed. Email: butler@chem.ucsb.edu.

This article contains supporting information online at https://www.pnas.org/lookup/suppl/doi:10.1073/pnas.2423730122/-/DCSupplemental.

Published March 3, 2025.

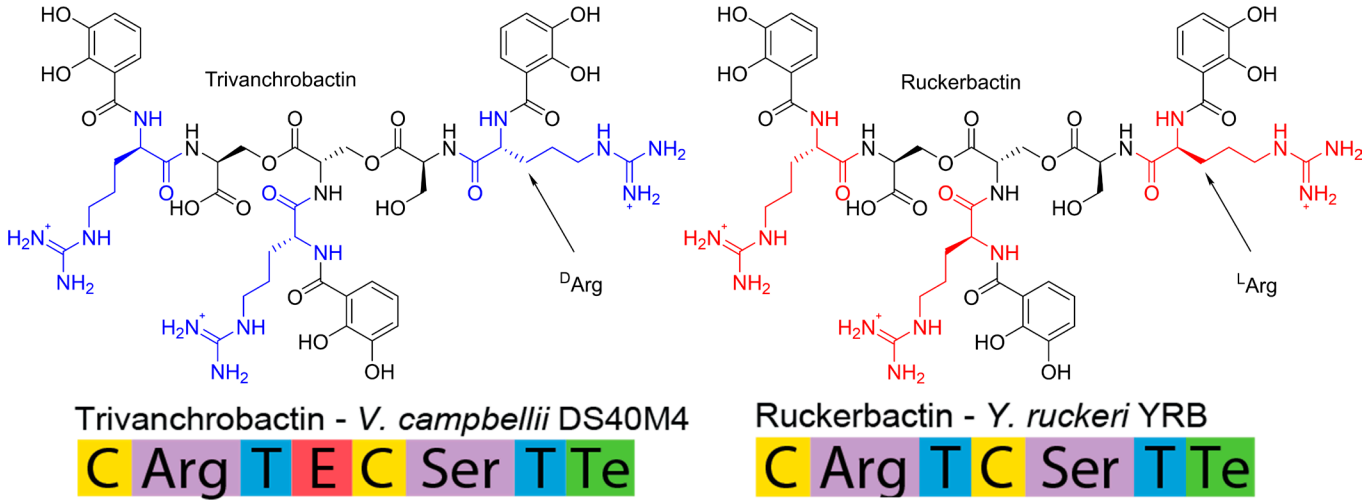

Fig. 1. Structures of the trivanchrobactin and ruckerbactin siderophores. Schematic of nonribosomal peptide synthetases (NRPS) in trivanchrobactin and ruckerbactin biosynthetic gene clusters (BGCs). NRPS abbreviations: C—condensation domain, T—thiolation domain, E—epimerase domain, Te—thioesterase domain; the domains indicated by Arg and Ser are the adenylation (A) domains.

nosocomial pathogen *Yersinia frederiksenii* ATCC 33641, respectively, are nearly diastereomeric with ^{D}Lys versus ^{L}Lys, except that the former is based on the tri-^{L}Ser macrolactone, whereas the latter has the linear tri-^{L}Ser scaffold (*SI Appendix*, Fig. S1) (14, 15). The nonribosomal peptide synthases (NRPSs) in the BGCs responsible for the biosynthesis of these siderophores (Fig. 1) function by loading the ^{L}CAA specified by the adenylation (A) domain, appending 2,3-dihydroxybenzoic acid (DHB), and subsequently loading the conserved ^{L}Ser specified by the second A domain. The stereochemistry of the incorporated amino acids is dictated by the presence or absence of an epimerase (E) domain, which converts an ^{L}CAA to a ^{D}CAA (16). These NRPSs function iteratively in three successive rounds installing ^{L}Ser ester linkages between the DHB-$^{D/L}$CAA-^{L}Ser units. The siderophore is released from the thioesterase domain as the macrolactone or the linear tri-^{L}Ser siderophores. This family of (DHB-$^{D/L}$CAA-^{L}Ser)$_3$ siderophores is the first identified combinatoric suite of metal-binding ligands encoded in microbial genomes, raising questions regarding the effects of mismatched chirality on microbial growth and iron uptake.

The stereochemistry of the CAA in the (DHB-$^{D/L}$CAA-^{L}Ser)$_3$ siderophore suite imparts a configurational preference for a Δ or Λ stereoisomer upon Fe(III) coordination. Siderophores which incorporate ^{D}CAAs produce Λ Fe(III) complexes and those containing ^{L}CAAs form Δ complexes (12, 15). Siderophore ligands differing only by the stereochemistry of a single amino acid residue is a relatively small molecular change compared to the wide variation in structures across the broad class of siderophores. The systematic variation within three sets of related diastereomeric pairs of siderophores suggests bacteria have evolved to recognize not only the molecular composition within a siderophore but perhaps also the specific chirality of the Fe(III)-coordination complex.

We report herein stereospecific control of microbial growth mediated by chiral Fe(III)–siderophores. A siderophore-deficient mutant of *V. campbellii* DS40M4, which was constructed to prevent biosynthesis of the native catechol siderophores, grows on its native cationic triscatecholate siderophore, Λ-Fe(III)–trivanchrobactin, and the related synthetic Λ-Fe(III) complexes of cyclic trichrysobactin, ^{Cy}(DHB-^{D}Lys-^{L}Ser)$_3$ and ^{Cy}(DHB-^{D}Orn-^{L}Ser)$_3$. However, the diastereomeric Δ-Fe(III)–ruckerbactin complex and the related synthetic complexes which form Δ-Fe(III)-complexes do not support growth. In agreement with the growth assays, we show that iron uptake is stereoselective for the native siderophore Λ-Fe(III)–trivanchrobactin and is significantly attenuated for its diastereomer Δ-Fe(III)–ruckerbactin. Moreover, the PBP FvtB is stereoselective for Λ-Fe(III)–trivanchrobactin and is unable to bind and shuttle the misconfigured Δ-Fe(III)–ruckerbactin complex.

Results

Effects of Fe(III)–Siderophore Chirality on Bacterial Growth. *V. campbellii* DS40M4 produces three primary siderophores, trivanchrobactin, amphienterobactin, and anguibactin (*SI Appendix*, Fig. S2), all of which contain 2,3-DHB (17). To investigate the effects of Fe(III)–siderophore chirality on the growth of *V. campbellii* DS40M4, a mutant lacking the ability to synthesize 2,3-DHB and consequently its native catechol siderophores was constructed (*Materials and Methods*) (17). An overnight culture of *V. campbellii* DS40M4 Δ*aebA* was inoculated into a low-iron minimal medium containing 10 μM ethylenediamine-N,N'-bis(2-hydroxyphenylacetic acid) (EDDHA) to induce iron starvation. Under these conditions, *V. campbellii* DS40M4 Δ*aebA* does not grow unless provided with an exogenous source of iron that can be utilized by the bacterium. Ferric ammonium citrate (FAC), added as a positive control, was able to rescue growth of the siderophore-deficient knockout mutant (*SI Appendix*, Fig. S3). Triscatecholate compounds were pipetted onto the plates as the apo ligands which transchelate Fe(III) sequestered by EDDHA, owing to the significantly higher affinity of triscatecholate ligands for Fe(III) over polycarboxylate ligands. The addition of the native siderophore trivanchrobactin rescues growth in iron-starved conditions as expected (Fig. 2 *A*, #1), however, the diastereomeric siderophore ruckerbactin does not rescue growth (Fig. 2 *A*, #5). The results of these bacterial growth assays are the first example of chiral discrimination occurring between diastereomeric ferric siderophore complexes that are enantiomeric at the Fe(III) coordination site. Although it is evident that the Δ stereoisomer of Fe(III)–ruckerbactin does not support growth of *V. campbellii* DS40M4 Δ*aebA*, further investigation is necessary to elucidate the specific biological step in which chiral discrimination occurs.

Effect of Structural Variations in the Siderophore on Microbial Growth. To investigate whether the nature of the CAA side chain or the connectivity within the oligoserine backbone (i.e., triester macrolactone vs. linear di-ester) affects microbial growth, the siderophore cyclic trichrysobactin ^{Cy}(DHB-^{D}Lys-^{L}Ser)$_3$ produced by *D. chrysanthemi* EC16 and the cyclic analogs of the five additional

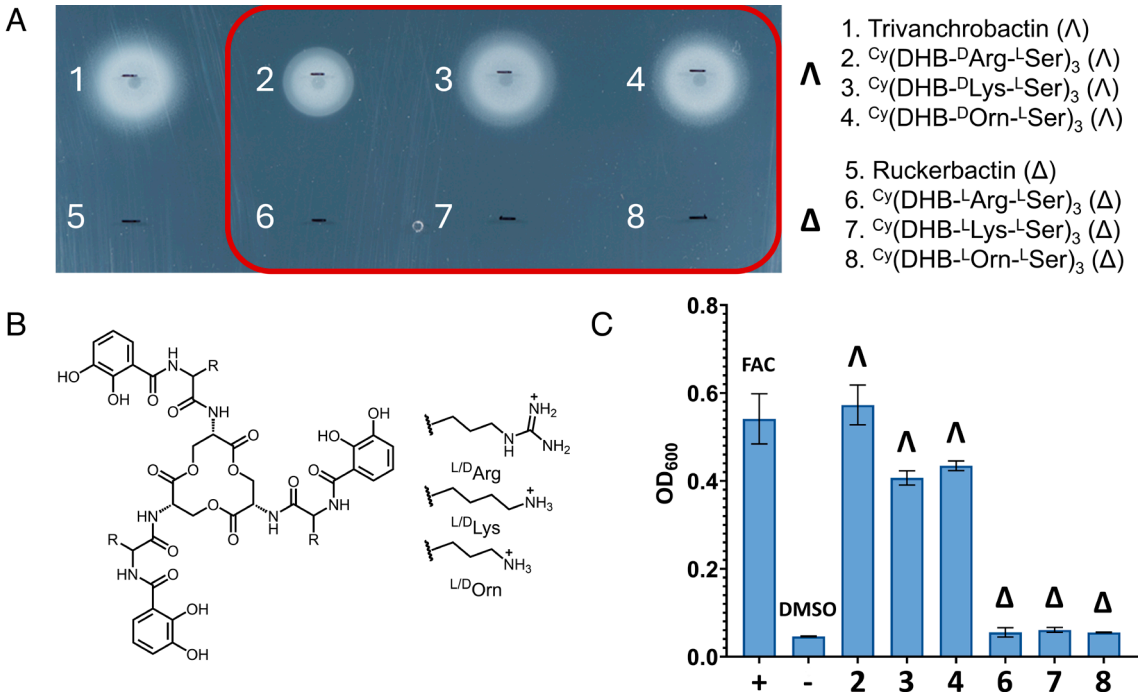

Fig. 2. Effect of Fe(III)-complex chirality on microbial growth. (*A*) Growth of *V. campbellii* DS40M4 Δ*aebA* on minimal agar medium supplemented with trivanchrobactin, ruckerbactin, and cyclic triscatecholate analogs with varying cationic amino acids (the configurations of the corresponding ferric complexes are indicated in parentheses). (*B*) Structure of the ^{Cy}(DHB-$^{L/D}$CAA-^{L}Ser)$_3$ suite of siderophore analogs, where CAA is $^{L/D}$Arg, $^{L/D}$Lys, or $^{L/D}$Orn. (*C*) Growth of *V. campbellii* DS40M4 Δ*aebA* in liquid media (AB media + 10 μM EDDHA) after 24 h of growth at 30 °C, 180 RPM. The indicated cyclic, cationic triscatecholate analogs were added at a final concentration of 10 μM and the SD of three independent trials are shown. Ferric ammonium citrate (FAC) was used as the positive control (+) and DMSO was used as both the negative control (−), as well as the solvent for the stock solutions.

linear siderophores containing CAAs [i.e., ^{Cy}(DHB-$^{L/D}$CAA-^{L}Ser)$_3$ where CAA is Arg, Lys, or Orn] (Fig. 2*B*) were synthesized (*SI Appendix*, Figs. S4–S11) and tested in bacterial growth assays. Chemical synthesis was employed to circumvent difficulties in isolating the relatively small amounts of the native siderophores from bacterial cultures and the analogs were synthesized in their macrocyclic form, utilizing preexisting methodology to form the tri-^{L}Serine macrolactone (18). Electronic circular dichroism (ECD) spectroscopy establishes that the configuration of the synthetic ferric complexes is consistent with the native siderophores (Fig. 3). Fe(III) complexes of ^{Cy}(DHB-^{L}Arg-^{L}Ser)$_3$, ^{Cy}(DHB-^{L}Lys-^{L}Ser)$_3$, and ^{Cy}(DHB-^{L}Orn-^{L}Ser)$_3$ give rise to ECD spectra that are the near mirror image of the corresponding Fe(III) complexes of ^{Cy}(DHB-^{D}Arg-^{L}Ser)$_3$, ^{Cy}(DHB-^{D}Lys-^{L}Ser)$_3$, and ^{Cy}(DHB-^{D}Orn-^{L}Ser)$_3$ (Fig. 3). Through comparison to the ECD spectra of the natural Fe(III)–siderophores and [Fe(III)-Ent]$^{3-}$, for which the absolute configuration is known (19), siderophore analogs containing an ^{L}CAA adjacent to the catecholate ligands are assigned as Δ Fe(III) complexes and their ^{D}CAA diastereomers form Fe(III) complexes of Λ configuration (19).

Bacterial growth assays carried out with the cyclic ^{Cy}(DHB-$^{L/D}$CAA-^{L}Ser)$_3$ suite of diastereomeric siderophore analogs reveal that the stereospecificity observed for the native siderophores is a general feature of the ferric trivanchrobactin uptake pathway. The synthetic cyclic form of trivanchrobactin induced growth of *V. campbellii* DS40M4 Δ*aebA* (Fig. 2 *A*, #2), whereas the cyclic version of ruckerbactin was unable to rescue growth (Fig. 2 *A*, #6), consistent with the corresponding native siderophores. Substitution of ^{D}Arg with either ^{D}Lys or ^{D}Orn, as in the compounds ^{Cy}(DHB-^{D}Lys-^{L}Ser)$_3$ and ^{Cy}(DHB-^{D}Orn-^{L}Ser)$_3$, also promotes growth of *V. campbellii* DS40M4 Δ*aebA*, however, no growth was observed for the corresponding diastereomers ^{Cy}(DHB-^{L}Lys-^{L}Ser)$_3$ and ^{Cy}(DHB-^{L}Orn-^{L}Ser)$_3$ (Fig. 2*A*). The results establish that microbial growth maintains a strict preference for the Λ configured Fe(III)–triscatecholate compounds with ^{D}CAAs and accommodates variation in the nature of the cationic amino acid side chain and the connectivity of the tri-^{L}serine backbone. Bacterial growth assays were replicated in liquid culture yielding analogous results (Fig. 2*C*). The triscatecholate ligands with ^{L}CAAs, which form Δ-Fe(III) complexes, uniformly did not promote growth under iron-starved conditions, while those that maintained the native Λ configuration of Fe(III)–trivanchrobactin promoted growth to a similar extent as the positive control FAC.

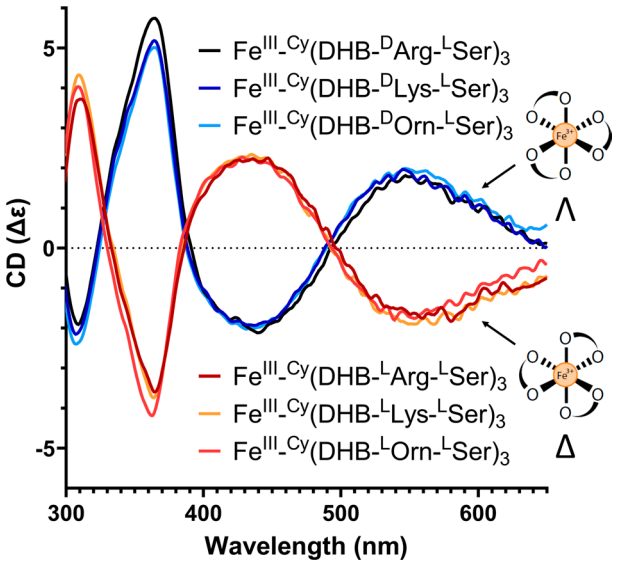

Fig. 3. Electronic circular dichroism (ECD) spectra for 50 μM solutions of the suite of Fe(III)–^{Cy}(DHB-CAA-^{L}Ser)$_3$ complexes in 50 mM bis-tris (pH 7.40).

Microbial Iron Uptake Mediated by ^{57}Fe(III)–Trivanchrobactin and ^{57}Fe(III)–Ruckerbactin. Intracellular import of an Fe(III)–siderophore across the outer membrane is the initial step in the biological pathway for iron uptake in many Gram-negative bacteria, with the siderophore OMR serving as the primary site of structural recognition. We determined the extent of microbial ^{57}Fe uptake mediated by trivanchrobactin and ruckerbactin by ICP-MS, which should account for uptake activity by any of the OMRs expressed by *V. campbellii* DS40M4. Cultures of *V. campbellii* DS40M4 Δ*aebA* were grown to exponential phase (OD_{600}: 0.60 ± 0.02) and equilibrated with either 5 μM ^{57}Fe(III)–trivanchrobactin or 5 μM ^{57}Fe(III)–ruckerbactin for 30 min at 30 °C, after which the cells were harvested, washed with a trace-metal-removing rinse (100 mM oxalate, 50 mM EDTA, 0.5% hydroxylamine hydrochloride), digested, and analyzed for ^{57}Fe content. ICP-MS measurements reveal that trivanchrobactin promoted a significant increase in intracellular ^{57}Fe relative to ruckerbactin and to control cultures to which no Fe(III)–siderophore complex was added. To account for differences in culture volume and to rule out the possibility that any elevated ^{57}Fe levels could be an artifact of differences in bacterial growth between samples, phosphorus levels were also measured by ICP-MS to determine the ratio of ^{57}Fe/P for each set of samples (Fig. 4*A*). Specifically, the ^{57}Fe/P ratio (mmol ^{57}Fe: mol P) of bacterial cultures with added ^{57}Fe(III)–trivanchrobactin increased 13-fold relative to the control culture, from 0.069 ± 0.005 to 0.91 ± 0.21, indicative of active uptake of ^{57}Fe. In contrast to ^{57}Fe(III)–trivanchrobactin-supplemented bacterial cultures, addition of 5 μM ^{57}Fe(III)–ruckerbactin to cultures of *V. campbellii* DS40M4 Δ*aebA* marginally increased the ratio of ^{57}Fe/P by only about three-fold relative to the control culture, from 0.069 ± 0.005 to 0.18 ± 0.09 (Fig. 4*A*).

The vanchrobactin OMR protein, FvtA, is encoded within the *V. campbellii* DS40M4 trivanchrobactin gene cluster and is likely the OMR for Fe(III)–trivanchrobactin. Additionally, genes encoding the amphi-enterobactin receptor FapA and the anguibactin receptor FatA are also present in the *V. campbellii* DS40M4 genome (*SI Appendix*, Fig. S12) (17, 20). Recognition of Fe(III)–ruckerbactin by any of these OMR proteins would result in an increase in the amount of cell-associated ^{57}Fe measured, as would nonspecific uptake or adventitious cell association. The ^{57}Fe/P ratio for cultures supplemented with ^{57}Fe(III)–ruckerbactin is only 20.1% of that of cultures incubated with the native ferric siderophore, ^{57}Fe(III)–trivanchrobactin, indicating that Fe(III)–siderophore uptake process is stereoselective. The results of the transport assays are consistent with the strong growth promotion by trivanchrobactin but do not fully account for the inability of *V. campbellii* DS40M4 Δ*aebA* to utilize ruckerbactin. Although siderophore uptake is strongly stereoselective in *V. campbellii*, chiral recognition by FvtA may not be the sole point of chiral discrimination within the Fe(III)–trivanchrobactin utilization pathway.

Fe(III)–siderophore Recognition by the PBP FvtB. Following intracellular import across the outer membrane, ferric triscatecholate complexes are bound by PBPs and delivered to ATP-binding cassette (ABC) transporters localized on the cytoplasmic membrane (7). The PBP FvtB has been found to be essential for growth of *Vibrio anguillarum* 775 (pJM1) on vanchrobactin (DHB-^{D}Arg-^{L}Ser), which is the monocatecholate analog of trivanchrobactin (DHB-^{D}Arg-^{L}Ser)$_3$ (20). A homolog of the *V. anguillarum* 775 (pJM1) *fvtB* gene (sequence identity, 56.6%) was identified in the genome of *V. campbellii* DS40M4 and expressed heterologously (*SI Appendix*, Fig. S13) to investigate whether chiral recognition occurs during periplasmic translocation of ferric triscatecholate siderophores to the cytoplasm. Notably, many ferric siderophore PBPs display configurational preference for Λ-Fe(III) complexes, as in the case of the tetradentate siderophore PBPs CeuE and VctP, which bind the Fe(III) complex of bis-(2,3-dihydroxybenzoyl-L-serine), Fe(III)–bisDHBS, and induce the Λ configuration (21, 22). Some Gram-negative bacteria additionally express periplasmic esterases, which hydrolyze the serine ester backbone prior to PBP binding and cytoplasmic import (23). Analysis of the *V. campbellii* DS40M4 genome for homologs of known cytoplasmic and periplasmic siderophore esterases reveals only a single cytoplasmic esterase that is homologous to the vanchrobactin esterase *vabH* (sequence identity, 58.9%) of *V. anguillarum* serovar O2 and which is located directly adjacent to the trivanchrobactin biosynthetic gene *vabF* (*SI Appendix*, Fig. S12) (24).

We hypothesized that the affinity of FvtB for Δ-Fe(III)– ruckerbactin would be low due to the mismatched configuration of the metal-complex relative to that of the native substrate Λ-Fe(III)–trivanchrobactin. Addition of the native ferric siderophore, Fe(III)–trivanchrobactin, to 250 nM FvtB results in strong quenching of the protein's intrinsic fluorescence (K_D 124.4 ± 8.7 nM) (Fig. 4*B*). However, addition of Fe(III)–ruckerbactin to 250 nM FvtB results in only minor fluorescence quenching (Fig. 4*B*). At 4 equivalents of Fe(III)–ruckerbactin to FvtB the normalized

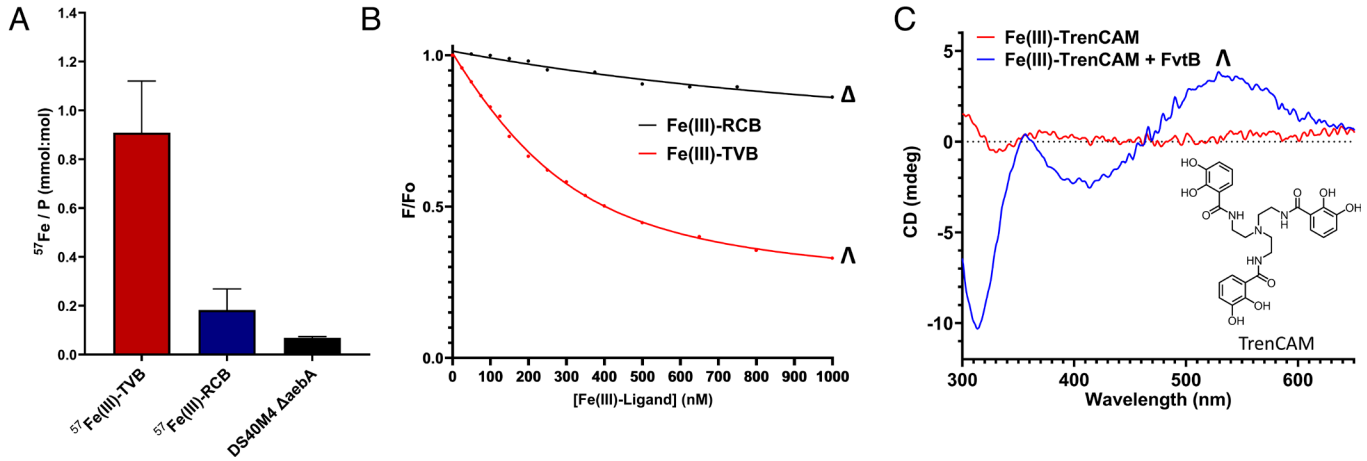

Fig. 4. Stereospecific recognition by Fe(III)–trivanchrobactin transport proteins. (*A*) ^{57}Fe/P ratio of bacterial cultures following incubation of *V. campbellii* DS40M4 Δ*aebA* with 5 μM of either ^{57}Fe(III)–trivanchrobactin (TVB, red) or ^{57}Fe(III)–ruckerbactin (RCB, blue) for 30 min at 30 °C. The baseline ^{57}Fe/P ratio for *V. campbellii* DS40M4 Δ*aebA* grown in AB medium without addition of a siderophore is indicated (black). (*B*) Fluorescence quenching (334 nm) of 250 nM FvtB as a function of Fe(III)–trivanchrobactin (red) or Fe(III)–ruckerbactin (black) concentration in 40 mM Tris (pH 7.50), 150 mM NaCl. (*C*) ECD spectra of 50 μM Fe(III)–TrenCAM in the absence (red) and presence (blue) of equimolar FvtB (40 mM Tris pH 7.50; 150 mM NaCl).

fluorescence decreases to only ~0.90, with an estimated K_D in the micromolar range (>3 μM).

The configurational preference of the FvtB binding pocket was further inferred through monitoring changes in the low-energy ECD bands of Fe(III)–TrenCAM (corresponding to ferric triscatecholate LMCT transitions) upon protein binding (Fig. 4*C*). The synthetic, achiral triscatecholate ligand TrenCAM forms a racemic mixture of Δ and Λ isomers in solution, as evinced by the featureless ECD spectrum (Fig. 4*C*). However, when a 50 μM solution of Fe(III)–TrenCAM is equilibrated with an equivalent concentration of FvtB, the ECD spectrum reveals the induction of strong CD bands indicating Λ chirality (Fig. 4*C*). Induction of Λ chirality in an otherwise racemic mixture of coordination isomers suggests that the FvtB binding pocket is predisposed to bind Λ-Fe(III)–triscatecholate complexes. Accordingly, the low binding affinity of FvtB for Δ-Fe(III)–ruckerbactin is likely a consequence of the mismatched configuration of the metal-complex relative to the shape of the binding pocket.

Although siderophore PBPs are often capable of inverting or inducing the coordination geometry around Fe(III) upon binding (21, 22), we hypothesize that the Δ configuration of Fe(III)–ruckerbactin precludes entrance into the binding pocket of FvtB, preventing Fe(III)–ruckerbactin from accessing key binding residues within the cleft. The extent of chiral recognition observed is notably much more pronounced than what has been reported previously for the Fe(III)–Ent PBP FepB, which binds both Δ-Fe(III)–Ent and the enantiomeric complex Λ-Fe(III)–Enantio-Ent with low nanomolar affinity. The stereoselectivity of FvtB may be a consequence of the positively charged Arg residues incorporated in the structures of both trivanchrobactin and ruckerbactin, as a result of their steric bulk and potential for electrostatic clashing. Consequently, a mispositioning of the bulky ^{L}Arg residues in Δ-Fe(III)–ruckerbactin could prevent the mismatched complex from associating sufficiently with FvtB.

Discussion

The genetically encoded suite of diastereomeric pairs of (DHB-$^{L/D}$CAA-^{L}Ser)$_3$ siderophores is a biologically produced combinatoric ligand set coordinating Fe(III) in opposing enantiomeric stereospecificity. Two of the siderophores, trivanchrobactin and ruckerbactin, are produced by the marine pathogens *V. campbellii* DS40M4 and *Y. ruckeri* YRB, respectively, which potentially live in the same environment. Their siderophores are diastereomeric, differing only by the presence of ^{D}Arg and ^{L}Arg and forming Λ and Δ Fe(III) complexes, respectively. Despite the similarity in ligand structures (Fig. 1), growth of *V. campbellii* DS40M4 Δ*aebA* is exquisitely selective for its endogenous siderophore, Λ-Fe(III)–trivanchrobactin, over the exogenous diastereomeric siderophore, Δ-Fe(III)–ruckerbactin (Fig. 2*A*). Certain structural variations, such as macrocyclization or substitution of ^{D}Arg with either ^{D}Lys or ^{D}Orn, all of which preserve the Λ configuration (Fig. 2*A*), retain the ability to promote growth of *V. campbellii* DS40M4 Δ*aebA*. However, substitution of ^{D}Arg for any ^{L}CAA abolishes growth promotion, consistent with the change from Λ to Δ stereochemistry. Uptake of iron is nearly as stereoselective as growth with Fe(III)–trivanchrobactin, although minimal ^{57}Fe is measured with Δ-Fe(III)–ruckerbactin (Fig. 4*A*). Nevertheless, if any Fe(III)–ruckerbactin were to cross the outer membrane, it does not bind to the PBP, FvtB (Fig. 4*B*), and thus cannot be transported into the cytoplasm, where iron release occurs for triscatecholate siderophores. Overall, the stereoselectivity highlights the remarkable specificity of some siderophore-binding proteins, where only a single inversion of stereochemistry is sufficient to abolish substrate recognition.

Chirality at the Fe(III) site and within the siderophore ligand has been of interest for decades, although relatively few examples of naturally occurring enantiomeric or diastereomeric siderophores are known. Pyochelin (*Pseudomonas aeruginosa*) and enantio-pyochelin (*Pseudomonas fluorescens* PAO1) are naturally produced enantiomers (25, 26). The pyochelin OMR, FptA, and the enantio-pyochelin receptor, FetA, are both stereoselective for their cognate enantiomer (27), as revealed in ligand binding and Fe(III)–siderophore uptake assays (28). The other identified natural enantiomeric pair is the bacterial siderophore *S,S*-rhizoferrin (*Ralstonia pickettii* DSM 6297) and the fungal siderophore, *R,R*-rhizoferrin (*Rhizopus microsporus var. rhizopodiformis*), of which less is known about stereoselective effects on microbial growth and iron uptake (29, 30).

Further investigations of siderophore chirality on microbial growth relied on the synthesis of siderophore enantiomers, which are not known to be naturally occurring (31–33). The synthetic enantiomer of enterobactin, ^{Cy}(DHB-^{L}Ser)$_3$, enantio-enterobactin, ^{Cy}(DHB-^{D}Ser)$_3$, containing an artificial tri-^{D}Ser macrolactone, is unable to rescue growth in iron-starved cultures of *E. coli* K12R (31). Despite decades of literature reports hypothesizing opposite configurations of Δ-Fe(III)–Ent and Λ-Fe(III)–Enantio-Ent as the basis of chiral discrimination in the ferric siderophore uptake pathway (31), Abergel et al. discovered that chiral recognition is imparted by the ferric enterobactin esterase Fes, which is unable to hydrolyze the synthetic tri-^{D}Ser macrolactone (9). Consequently, intracellular Fe(III)–Enantio-Ent builds up in the cytoplasm with no means for the bacterium to remove and utilize iron from the complex.

Unlike the previous examples of single enantiomeric pairs (25, 26), trivanchrobactin, ruckerbactin, and the four additional cationic triscatecholate siderophores of (DHB-$^{L/D}$CAA-^{L}Ser)$_3$ form a suite of naturally occurring diastereomeric pairs produced by distinct strains of bacteria. The diastereomeric pairs of siderophores coordinate Fe(III) in a stereoselective fashion to form metal-complexes of opposing Δ and Λ configuration, as a consequence of the CAA stereochemistry. The Λ-Fe(III)–trivanchrobactin-utilization pathway of the marine bacterium *V. campbellii* DS40M4 was found to be strictly stereoselective for Λ-Fe(III) siderophore complexes with ^{D}CAAs. Given the abundance of chiral triscatecholate siderophores encoded within microbial genomes (12), we suggest that privatization of iron can be driven through modulating the coordination isomerism of a ferric siderophore complex. The ecological benefits of siderophore privatization have been directly demonstrated in natural *Pseudomonad* communities, where a fitness advantage was observed for producers of unique pyoverdine variants that were not recognized by the canonical pyoverdine receptors of nonproducing strains (5). With regard to the present study, the stereoselectivity of the trivanchrobactin uptake pathway would serve to benefit *Y. ruckeri* YRB, as any ruckerbactin produced would be unable to be effectively utilized by competing *Vibrio* strains expressing ferric trivanchrobactin uptake proteins.

With chirality established as a mechanism for iron siderophore privatization, microbes may have evolved to control chirality in other secondary metabolites as a means of privatization. The BGCs of the combinatoric suite of triscatecholate siderophores presented herein are found in a diverse array of microbial genomes, hinting at the existence of other BGCs encoding enantiomeric or diastereomeric natural products. Site-specific chirality can often be predicted using bioinformatic tools, particularly in the case of NRPS-derived metabolites, which utilize readily identifiable epimerase domains to control the stereochemistry of amino acid building blocks. Consequently, microbial genome screening for enantiomeric or diastereomeric peptidic natural products is facile and may enable the discovery of new ecologically important chiral metabolites.

Materials and Methods

Bacterial Strains. A siderophore-deficient knockout strain, *V. campbellii* DS40M4 Δ*aebA* was obtained as previously described (17). *V. campbellii* DS40M4 Δ*aebA* was routinely maintained on plates composed of Difco™ marine broth 2216 media + 1.5% agar. Overnight cultures were grown through inoculation of a single colony into 2216 media and grown at 30 °C, 180 RPM overnight.

General Methods. All reactions performed under an argon atmosphere were carried out using a high-vacuum line, standard Schlenk techniques, and dry solvents. DMF, DCM, and DMSO-d_6 were stored over 3 Å molecular sieves for at least 72 h prior to use. *N,N*-diisopropylethylamine (DIPEA) was purified by distillation over ninhydrin (x3) and was subsequently stored over 3 Å molecular sieves. Isotopically enriched ^{57}Fe (>95%) was obtained from Cambridge Isotopes Laboratories. All protected amino acid starting materials were obtained from Bachem. All other reagents were purchased from Sigma-Aldrich. Milli-Q® water from a Milli-Q® IQ 7000 water purification system (Resistivity 18.2 MΩ cm) was used for the preparation of bacterial media, preparation of all stock solutions, and for all ICP-MS experimental work.

Synthesis of Cyclic Analogs of the Native Triscatecholate Siderophores. The cyclic analogs of the native triscatecholate siderophores were synthesized as described previously for the triscatecholate siderophore cyclic trichrysobactin (15). Synthesis of arginine-containing compounds utilized either N_α-Boc-N_δ,N_ω-di-Z-L-arginine (Bachem) or N_α-Boc-N_δ,N_ω-di-Z-D-arginine (Bachem) as starting materials. Ornithine-containing compounds analogously utilized either N_α-Boc-N_δ-Z-L-ornithine or N_α-Boc-N_δ-Z-D-ornithine as starting materials. The stereochemistry of the macrolactone was controlled by using N_α-trityl-L-serine methyl ester as the starting material for macrolactonization following established literature procedures (18).

^{13}C NMR spectroscopy was performed on a Bruker Advanced Neo 500 MHz spectrometer equipped with a prodigy cryoprobe at RT. All ^{1}H, COSY, HMBC, HSQC NMR spectroscopy was performed on a Varian Unity 600 MHz spectrometer at RT. Chemical shifts were referenced through residual solvent peaks [^{1}H (DMSO-d_6) 2.50 ppm, ^{13}C (DMSO-d_6) 39.51 ppm]. HR-ESIMS analysis of synthetic compounds was carried out on a Waters LCT Premier ESI TOF introduced into the ESI by direct infusion via a syringe pump.

Isolation of Ruckerbactin and Trivanchrobactin. Ruckerbactin was isolated from cultures of *Y. ruckeri* YRB as previously described (11). Trivanchrobactin was isolated through hydrolysis of the synthetic cyclic congener, (DHB-^{D}Arg-^{L}Ser)$_3$. Aqueous hydrolysis was carried out through dissolution of (DHB-^{D}Arg-^{L}Ser)$_3$ in MOPS buffer (50 mM, pH 7.40) and allowed to gently stir at room temperature for 24 h, at which point the cyclic trilactone starting material is only faintly detectable by HPLC. The resulting hydrolysis products were separated using semipreparative RP-HPLC on a YMC-Actus 20 × 250 mm C18 ODS-AQ column using a linear gradient of 10 to 30% ACN (+0.05% TFA) in H_2O (+0.05% TFA) over 30 min (*SI Appendix*, Fig. S14). Peaks were collected manually and concentrated for subsequent ESI-MS characterization (*SI Appendix*, Fig. S15).

Preparation of Fe(III)–siderophore and ^{57}Fe(III)–siderophore complexes. Ferric chloride hexahydrate (0.125 mmol) was dissolved in 50 mL of 0.05 M HCl (aq.) to obtain a final concentration of approximately 2.5 mM. The resulting solution was standardized spectrophotometrically using 1,10-phenathroline [ε_{511nm} $Fe^{II}(1,10\text{-Phen})_3$ 11,100 cm^{-1} M^{-1}] (34). Fe(III)–complexes of the siderophore analogs were prepared in bis-tris buffer (50 mM, pH 7.40) by mixing a solution of $FeCl_3$ [2.45 mM, 0.05 M HCl (aq.)] with 1.0 equivalent of the desired apo-ligand. The formation of the Fe(III)–complex was tracked by UV-visible spectroscopy by observing an increase in the absorbance at 498 nm. The resulting solution was equilibrated at room temperature for 30 min prior to analysis by CD spectroscopy.

A stock solution of $^{57}Fe(NO_3)_3$ was prepared through dissolution of ~10 mg metallic ^{57}Fe powder (Cambridge Isotopes Laboratory, >95%) in 10 ml of refluxing 30% HNO_3 for 24 h. Following dilution with an equivalent volume of water, the concentration was standardized spectrophotometrically with 1,10-phenanthroline. ^{57}Fe(III)–siderophores for isotopic studies were prepared through equilibration of 1.2 equivalents triscatecholate siderophore and 1.0 molar equivalents of $^{57}Fe(NO_3)_3$ in bis-tris buffer (50 mM, pH 7.00).

Bis-tris buffer was used in all assays due to its weak metal-binding properties. Fe(III)–triscatecholate complexes form rapidly in bis-tris buffer at physiological pH (<15 min).

Circular Dichroism Spectroscopy. CD spectra were obtained in 50 mM bis-tris buffer (pH 7.40) at a concentration of 50 μM. Full CD spectra were acquired on a Jasco J-1500 spectrophotometer using the following parameters: 4 s D.I.T., 1 nm bandwidth, 50 nm/min scanning speed, with 3 accumulations. Units were converted from millidegrees (m°) to molar extinction coefficient (ε) through the following conversion: $\varepsilon = \frac{m^\circ}{(c)(l)(32{,}980)}$.

Bacterial Growth Assays. The Δ*aebF* in-frame deletion mutant was constructed following the literature procedure (35), using the following primers:

aebA-mut-SpeI-F: ACTAGTGAGTTACGAAGCATAATTATCTCTCAAGC

aebA-mut-SmaI-1: GTTAACTTTCCGTTCGGCGGAGGCTCACCCGGGCATTCCTTTCT CCTTTTGTGCAACAAG

aebA-mut-SmaI-2: CTTGTTGCACAAAAGGAGAAAGGAATGCCCGGGTGAGCCTCC GCCGAACGGAAAGTTAAC

aebA-mut-SacI-R: GAGCTCAATATAGACCCAAACCATCTAATG

An overnight culture of *V. campbellii* DS40M4 Δ*aebA* was inoculated into AB media containing warm agar (0.75% w/v) and 10 μM ethylenediamine-N,N′-bis(2-hydroxyphenyl-acetic acid) (EDDHA) to induce iron starvation. Sterile AB medium was prepared through dissolution of NaCl (17.5 g), $MgSO_4$ (12.3 g), and casamino acids (2.0 g) in 960 mL of Milli-Q® H_2O. The pH of this mixture was adjusted to 7.5 with 1 M NaOH and subsequently autoclaved. Preparation of the medium was completed through the addition of sterile stocks of 50% glycerol (20 mL), 1 M potassium phosphate (pH 7.0, 10 mL), and 0.1 M L-arginine (10 mL). Siderophore utilization assays were performed by aliquoting DMSO stocks (2 μL, 1 mM) of the analytes onto preinoculated AB media agar plates and successful siderophore utilization was indicated by the presence of zones of bacterial growth. Plates were grown at 30 °C for approximately 48 h prior to photographing.

For liquid growth promotion assays, overnight cultures of DS40M4 Δ*aebA* were inoculated into AB media (198 μL per well) containing 10 μM EDDHA. Siderophore utilization assays were performed by aliquoting DMSO stocks (2 μL, 1 mM) of the analytes into each well to reach a final concentration of 10 μM siderophore. The 96-well plates were sealed with a permeable membrane and allowed to grow at 30 °C, 180 RPM for 24 h. Growth was quantified using a Tecan Spark 10 M Multimode plate reader to measure the absorbance at 600 nm. Experiments were carried out in triplicate.

ICP-MS ^{57}Fe(III)–siderophore Uptake. An overnight culture of *V. campbellii* DS40M4 Δ*aebA* in 2216 media was diluted 400x fold into sterile AB media. The culture was subsequently grown at 30 °C, 180 RPM to an OD_{600} of 0.60 ± 0.02, at which point 10 mL aliquots of bacterial culture were transferred to 15 mL conical tubes. Bacterial cells were pelleted and the spent media was decanted. Bacterial pellets were brought up in 10 mL of fresh media supplemented with 5 μM ^{57}Fe(III)–siderophore or DMSO as a control. ^{57}Fe(III)–siderophore complexes were prepared in a 1.2:1.0 ratio of siderophore to $^{57}Fe(NO_3)_3$ and allowed to equilibrate for 30 min. The 50 μM stock solutions of the ^{57}Fe(III)–siderophore complexes were filtered twice through 0.22-μm syringe filters (MilliporeSigma™ Millex™-GS Syringe Filter Unit) to remove trace amounts of precipitate that interfered with the interpretation of the ICP-MS measurements (*SI Appendix*, Figs. S16 and S17). Following filtration, the concentration of the stock solutions was determined using the molar extinction coefficients of the Fe(III)–siderophore complexes ($\varepsilon_{498\,nm}$) and the appropriate amount of stock solution was pipetted into bacterial cultures to reach a final concentration of 5 μM. Each condition was carried out in triplicate and allowed to equilibrate with the bacterial culture through incubation at 30 °C, 180 RPM for 30 min. Cells were subsequently harvested on 0.40 μm polycarbonate filters (MilliporeSigma™ Isopore™) and rinsed with 10 mL AB media, followed by 10 mL of a trace metal rinse consisting of 100 mM oxalate, 50 mM EDTA, and 0.05% hydroxylamine hydrochloride (pH 8.00).

Filters containing the harvested cells were digested overnight at 110 °C in 50% nitric acid (TraceSELECT™ Ultra, Honeywell Fluka). The following morning, digestion vials were allowed to cool to room temperature, opened to the atmosphere, and then heated at 100 °C until approximately 10 μL of solution remained. Then, 100 μL of nitric acid was added to each vial and then the vials were gently heated until approximately 10 μL of solution remained. The digestions were subsequently brought up in 3 mL of ICP-MS solution containing 5% nitric acid and a 10 ppb Indium ICP-MS standard in Milli-Q® H_2O. Digestions were refluxed for 8 h, filtered, and analyzed by ICP-MS.

The following elements were monitored on standard mode, and quantification was performed by an external calibration using a 5-point standard curve: ^{31}P, ^{57}Fe, ^{113}In. The standards were prepared by serial dilution of 10 ppm CMS-3 and 71-A

multiple element standards (Inorganic Ventures) to final concentrations of 0.1, 1, 10, 100, and 1,000 ppb. The limit of detection for the instrument, as three times the SD of the acid blank (2% HNO_3, v/v), was 26 and 0.15 ppb for P and ^{57}Fe, respectively. The average vial blank correction to our samples was 0% and 4% for each element P and ^{57}Fe, respectively.

The process of rinsing was determined to add 7.20 ± 0.42 ng of ^{57}Fe, or ~1.9 times the concentration of the filter blank (3.71 ± 0.39 ng of ^{57}Fe). Referred to as the "process blank," this correction, which includes the blanks of the rinse solutions, filter, and acid blanks, was significant for the ruckerbactin treatment (correction of 30 ± 9% of ^{57}Fe measurement) compared to the trivanchrobactin treatment (7 ± 1%). The excellent precision on the "process blanks" means we confidently make these corrections to our data.

Expression and Purification of Hisx8-FvtB. FvtB containing an N-terminal Hisx8 tag and a TEV protease cleavage site was obtained from Twist Bioscience on a pET-28b plasmid. The plasmid was transformed into chemically competent *E. coli* BL21(DE3) and grown on LB agar + kanamycin. For expression of FvtB, a single colony was picked into LB + Kan (0.05%) and grown overnight. The overnight culture was inoculated into 2 L of fresh LB + Kan and grown until an OD_{600} of 0.60 to 0.80 was obtained. The culture was immediately taken out of the incubator upon reaching this stage of growth and allowed to cool to room temperature for 15 to 30 min. A freshly prepared sterile stock of IPTG was then added to induce expression of FvtB at a final concentration of 0.5 mM. Protein expression was conducted for 20 h at room temperature on an orbital shaker.

The following day the cells were harvested through centrifugation (6,000 RPM, 0 °C, 30 min), and the spent supernatant was discarded. Cell pellets were subsequently transferred to 50 mL centrifuge tubes, brought up in a minimal amount of lysis buffer, and stored at −80 °C for a minimal period of 24 h. For cell lysis, the harvested cells were thawed on ice and diluted with lysis buffer up to 40 mL per 2 L of culture. Lysozyme and protease inhibitor (phenylmethylsulfonyl fluoride) were added and the cells were lysed via sonication. Cell debris was removed through centrifugation and proteins were purified from the cell lysate through equilibration with 2 mL of fresh Ni-NTA resin (1 h, 4 °C, 180 RPM). The resin was subsequently loaded onto a column and rinsed with lysis buffer containing an increasing amount of imidazole (15 mM, 50 mM, 250 mM, and 500 mM) in order to elute the protein of interest. Fractions were collected and analyzed through SDS-PAGE (*SI Appendix*, Fig. S13). Fractions containing His-FvtB (MW: 34.1 kDa) were concentrated using 10,000 MW cutoff centrifugal filters (Amicon® Ultra-15) and exchanged into tris-buffered saline (TBS) using BioRad Econo-Pac 10G desalting columns.

The molar extinction coefficient at 280 nm was estimated by taking the difference spectrum of FvtB dissolved in 6 M guanidine at pH 12.50 relative to a 6 M guanidine solution of FvtB at pH 7.10 (36). The concentration of protein dissolved in solution under these conditions can be approximated using the following relationship: $[\text{protein}]\,(\text{mg/mL}) = \frac{A(280nm)}{2{,}357Y + 830W}$, where Y and W are equivalent to the number of tyrosine and tryptophan residues, respectively.

FvtB Fe(III)–Siderophore Binding Assays. All in vitro assays were conducted in Tris-buffered saline (pH 7.50) consisting of 150 mM NaCl and 40 mM Tris buffer at room temperature. Protein stock solutions consisting of 25% glycerol were stored at −20 °C and fresh solutions of FvtB were prepared daily prior to experiments through dilution of the glycerol stock into Tris-buffered saline. The absorbance at 280 nm in Tris-buffered saline was used to estimate the concentration of FvtB. All fluorescence spectra were recorded using an Agilent Cary Eclipse fluorescence spectrophotometer. Fluorescence quenching assays were recorded using the simple reads application and the following parameters: $\lambda_{excitation}$: 280 nm, $\lambda_{emission}$: 334 nm, average time: 2 s, Voltage: 850 mV. The spectrophotometer was blanked prior to each set of runs using buffer in a quartz cuvette. Each sample consisted of a 250 nM solution of FvtB in Tris-buffered saline and the appropriate concentration of analyte. Solutions containing a final volume of 3 mL were mixed by gently inverting the cuvette three times and were equilibrated for 5 min prior to recording the fluorescence. The data were plotted as the normalized fluorescence (the fluorescence of each sample normalized by the fluorescence of 250 nM FvtB in the absence of ligand) (*SI Appendix*, Figs. S18 and S19).

Ferric complexes were prepared by mixing a standardized stock solution of $FeCl_3$ (2.45 mM) with an equimolar amount of ligand in tricine buffer (50 mM, pH 7.50). Solutions were prepared as 10 μM working stocks and allowed to equilibrate for 15 min prior to fluorescence quenching assays. Fluorescence quenching curves were achieved by preparing a series of individual samples containing 250 nM FvtB and a varying concentration of ferric complexes, spanning a range of 0.1 equivalents–4.0 equivalents of analyte with respect to FvtB. Quenching data were inputted into Dynafit (37), and K_D values were computed based on the data assuming a fixed concentration of FvtB (250 nM).

ECD Spectroscopy. A fresh solution of ~100 μM FvtB was removed from a −80 °C freezer prior to use and allowed to thaw on ice. The concentration of the FvtB solution was estimated using the calculated molar extinction coefficient at 280 nM (ε 38,240 $cm^{-1}\,M^{-1}$). Fe(III)–siderophore (500 μL of a 100 μM 2× stock) was mixed with the appropriate volume of FvtB to achieve a final concentration of 50 μM FvtB and a total volume of 1 mL. The 1:1 FvtB:Fe(III)–siderophore solution was equilibrated for 15 min and analyzed by CD spectroscopy (*SI Appendix*, Fig. S20).

Data, Materials, and Software Availability. All study data are included in the article and/or *SI Appendix*.

ACKNOWLEDGMENTS. This work was supported by NSF Grants CHE-2108596 (A.B.), OCE-0838213 (M.G.H.), OCE-2049301 (K.A.B.), and NSF Postdoctoral Fellowship Grant OCE-2126562 (K.O.F.).

Author affiliations: [a]Department of Chemistry and Biochemistry, University of California, Santa Barbara, CA 93106; [b]Geosciences Research Division, Scripps Institution of Oceanography, University of California San Diego, La Jolla, CA 92093; and [c]Department of Medicinal Chemistry, University of Utah, Salt Lake City, UT 84112

1. I. J. Schalk, Bacterial siderophores: Diversity, uptake pathways and applications. *Nat. Rev. Microbiol.* **23**, 24–40 (2025).
2. Y. Zhang, S. Sen, D. P. Giedroc, Iron acquisition by bacterial pathogens: Beyond tris-catecholate complexes. *ChemBioChem* **21**, 1955–1967 (2020).
3. C. C. Murdoch, E. P. Skaar, Nutritional immunity: The battle for nutrient metals at the host–pathogen interface. *Nat. Rev. Microbiol.* **20**, 657–670 (2022).
4. R. Niehus, A. Picot, N. M. Oliveira, S. Mitri, K. R. Foster, The evolution of siderophore production as a competitive trait. *Evolution* **71**, 1443–1455 (2017).
5. E. Butaitė, M. Baumgartner, S. Wyder, R. Kümmerli, Siderophore cheating and cheating resistance shape competition for iron in soil and freshwater Pseudomonas communities. *Nat. Commun.* **8**, 414 (2017).
6. Z. L. Reitz, M. H. Medema, Genome mining strategies for metallophore discovery. *Curr. Opin. Biotech.* **77**, 102757 (2022).
7. T. E. Clarke, S.-Y. Ku, D. R. Dougan, H. J. Vogel, L. W. Tari, The structure of the ferric siderophore binding protein FhuD complexed with gallichrome. *Nat. Struct. Biol.* **7**, 287–291 (2000).
8. I. Josts, K. Veith, V. Normant, I. J. Schalk, H. Tidow, Structural insights into a novel family of integral membrane siderophore reductases. *Proc. Natl. Acad. Sci. U.S.A.* **118**, e2101952118 (2021).
9. R. J. Abergel, A. M. Zawadzka, T. M. Hoette, K. N. Raymond, Enzymatic hydrolysis of trilactone siderophores: Where chiral recognition occurs in enterobactin and bacillibactin iron transport. *J. Am. Chem. Soc.* **131**, 12682–12692 (2009).
10. M. Sandy *et al.*, Vanchrobactin and Anguibactin Siderophores Produced by *Vibrio* sp DS40M4. *J. Nat. Prod.* **73**, 1038–1043 (2010).
11. E. Thomsen, Z. L. Reitz, P. R. Stow, K. Dulaney, A. Butler, Ruckerbactin produced by *Yersinia ruckeri* YRB is a diastereomer of the Siderophore Trivanchrobactin produced by *Vibrio campbellii* DS40M4. *J. Nat. Prod.* **85**, 264–269 (2022).
12. A. Butler *et al.*, Mining elements of siderophore chirality encoded in microbial genomes. *Febs Lett.* **597**, 134–140 (2023).
13. A. W. Han *et al.*, Turnerbactin, a novel triscatecholate siderophore from the shipworm endosymbiont *Teredinibacter turnerae* T7901. *Plos One* **8**, e76151 (2013).
14. M. Sandy, A. Butler, Chrysobactin Siderophores produced by *Dickeya chrysanthemi* EC16. *J. Nat. Prod.* **74**, 1207–1212 (2011).
15. P. R. Stow, Z. L. Reitz, T. C. Johnstone, A. Butler, Genomics-driven discovery of chiral triscatechol siderophores with enantiomeric Fe(III) coordination. *Chem. Sci.* **12**, 12485–12493 (2021).
16. Z. L. Reitz, M. Sandy, A. Butler, Biosynthetic considerations of triscatechol siderophores framed on serine and threonine macrolactone scaffolds. *Metallomics* **9**, 824–839 (2017).
17. H. Naka, Z. L. Reitz, A. L. Jelowicki, A. Butler, M. G. Haygood, Amphi-enterobactin commonly produced among *Vibrio campbellii* and *Vibrio harveyi* strains can be taken up by a novel outer membrane protein FapA that also can transport canonical Fe(III)-enterobactin. *JBIC J. Biol. Inorg. Chem.* **23**, 1009–1022 (2018).
18. R. J. A. Ramirez, L. Karamanukyan, S. Ortiz, C. G. Gutierrez, A much improved synthesis of the siderophore enterobactin. *Tetrahedron Lett.* **38**, 749–752 (1997).
19. T. C. Johnstone, E. M. Nolan, Determination of the molecular structures of ferric enterobactin and ferric enantioenterobactin using racemic crystallography. *J. Am. Chem. Soc.* **139**, 15245–15250 (2017).
20. H. Naka, M. Q. Liu, J. H. Crosa, Two ABC transporter systems participate in siderophore transport in the marine pathogen *Vibrio anguillarum* 775 (pJM1). *Fems Microbiol. Lett.* **341**, 79–86 (2013).
21. D. J. Raines *et al.*, Bacteria in an intense competition for iron: Key component of the Campylobacter jejuni iron uptake system scavenges enterobactin hydrolysis product. *Proc. Natl. Acad. Sci. U.S.A.* **113**, 5850–5855 (2016).
22. E. J. Wilde *et al.*, Mimicking salmochelin S1 and the interactions of its Fe(III) complex with periplasmic iron siderophore binding proteins CeuE and VctP. *J. Inorg. Biochem.* **190**, 75–84 (2019).

23. X. Zeng, Y. Mo, F. Xu, J. Lin, Identification and characterization of a periplasmic trilactone esterase, Cee, revealed unique features of ferric enterobactin acquisition in ampylobacter. *Mol. Microbiol.* **87**, 594–608 (2013).
24. M. Balado, C. R. Osorio, M. L. Lemos, A gene cluster involved in the biosynthesis of vanchrobactin, a chromosome-encoded siderophore produced by *Vibrio anguillarum*. *Microbiol.* **152**, 3517–3528 (2006).
25. C. D. Cox, K. L. Rinehart Jr., M. L. Moore, J. C. Cook Jr., Pyochelin: Novel structure of an iron-chelating growth promoter for *Pseudomonas aeruginosa*. *Proc. Natl. Acad. Sci. U.S.A.* **78**, 4256–4260 (1981).
26. Z. A. Youard, G. L. A. Mislin, P. A. Majcherczyk, I. J. Schalk, C. Reimmann, Pseudomonas fluorescens CHA0 Produces Enantio-pyochelin, the Optical Antipode of the *Pseudomonas aeruginosa* Siderophore Pyochelin*. *J. Biol. Chem.* **282**, 35546–35553 (2007).
27. F. Hoegy *et al.*, Stereospecificity of the siderophore pyochelin outer membrane transporters in fluorescent pseudomonads. *J. Biol. Chem.* **284**, 14949–14957 (2009).
28. K. Brillet *et al.*, Pyochelin enantiomers and their outer-membrane siderophore transporters in fluorescent pseudomonads: structural bases for unique enantiospecific recognition. *J. Am. Chem. Soc.* **133**, 16503–16509 (2011).
29. M. Münzinger *et al.*, S, S-rhizoferrin (enantio-rhizoferrin)–A siderophore of *Ralstonia* (*Pseudomonas*) *pickettii* DSM 6297–The optical antipode of R. R-rhizoferrin isolated from fungi. *Biometals* **12**, 189–193 (1999).
30. H. Drechsel, G. Jung, G. Winkelmann, Stereochemical characterization of rhizoferrin and identification of its dehydration products. *Biometals* **5**, 141–148 (1992).
31. J. B. Neilands, T. J. Erickson, W. H. Rastetter, Stereospecificity of the ferric enterobactin receptor of Escherichia coli K-12. *J. Biol. Chem.* **256**, 3831–3832 (1981).
32. G. Winkelmann, V. Braun, Stereoselective recognition of ferrichrome by fungi and bacteria. *Fems Microbiol. Lett.* **11**, 237–241 (1981).
33. G. Müller, Y. Isowa, K. N. Raymond, Stereospecificity of siderophore-mediated iron uptake in *Rhodotorula pilimanae* as probed by enantiorhodotorulic acid and isomers of chromic rhodotorulate. *J. Biol. Chem.* **260**, 13921–13926 (1985).
34. N. Rajendraprasad, K. Basavaiah, Highly sensitive spectrophotometric determination of olanzapine using cerium(IV) and iron(II) complexes of 1,10-phenanthroline and 2,2′-bipyridyl. *J. Anal. Chem.*+ **65**, 482–488 (2010).
35. H. K. Zane *et al.*, Biosynthesis of amphi-enterobactin siderophores by *Vibrio harveyi* BAA-1116: Identification of a bifunctional nonribosomal peptide synthetase condensation domain. *J. Am. Chem. Soc.* **136**, 5615–5618 (2014).
36. N. J. Greenfield, Using circular dichroism spectra to estimate protein secondary structure. *Nat. Protocols* **1**, 2876–2890 (2006).
37. P. Kuzmič, "Chapter 10–DynaFit–A software package for enzymology" in *Methods in Enzymology*, M. L. Johnson, L. Brand, Eds. (Academic Press, 2009), **vol. 467**, pp. 247–280.